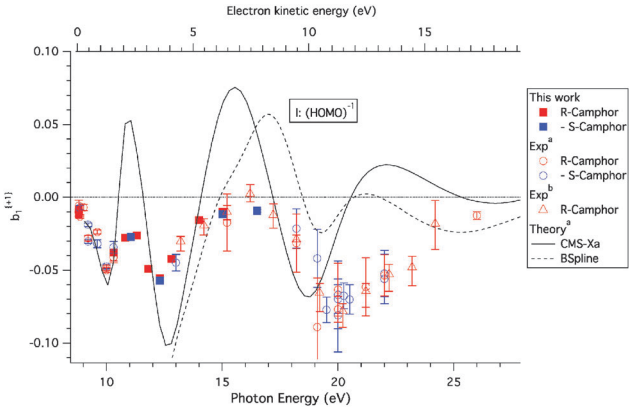

Fig. 3 Mean chiral parameter (b_1) for ionization of the HOMO orbital of camphor obtained at different photon energies. The markers represent experimental measurements while the lines correspond to two different scattering models. The *S*-enantiomer data have been negated. For some of the data points, the statistical error bars are not visible because they are smaller than the point width (see Table S1, ESI†). The values in this work have been normalized by S_3 and the ee measured by GC × GC-TOFMS. [a] From ref. 36. [b] From ref. 35.

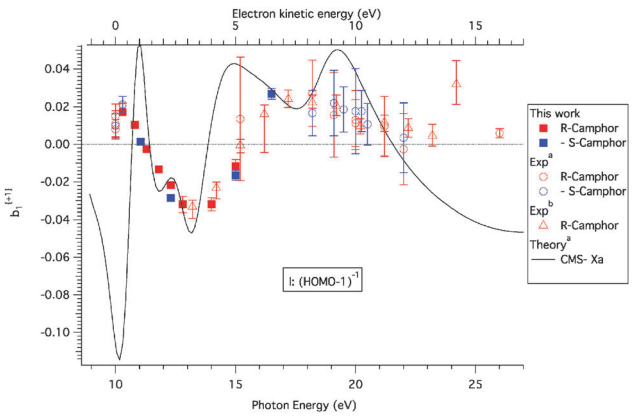

Fig. 4 Mean chiral parameter (b_1) for ionization of the HOMO−1 orbital of camphor, corresponding to the binding energy region 10–10.3 eV, obtained at different photon energies. The markers represent experimental measurements while the line correspond to the CMS-Xα scattering models. The *S*-enantiomer data have been negated. For some of the data points, the statistical error bars are not visible because they are smaller than the point width (see Table S1, ESI†). The values in this work have been normalized by S_3 and the ee measured by GC × GC-TOFMS. [a] From ref. 36. [b] From ref. 35.

proportional to S_3. A low absolute value of S_3 will at best—when it is known—lead to a decreased sensitivity to chirality by increasing the error bar on b_1 and, at worst—if not recognized—lead to incorrect PECD amplitudes. The argument must be also extended to cases where the Stokes parameters S_1 and S_2 defining respectively the linear polarization rates with respect to normal and 45° tilted axis, are non-zero. In such cases, if the usual anisotropy parameter β is non-zero, the S_1 and S_2 contributions to the photoelectron angular distribution (PAD) need to be taken into account. This would be a severe issue in the case of a VMI spectrometer relying on Abel inversion of a 2D image (*i.e.* without electron time-of-flight available to provide a direct 3D momentum determination) since only the cases where the axis of symmetry given by the light's polarization state is contained within the detector plane can be properly treated. However, in the case of the present experiments, the DESIRS beamline delivers quasi-perfect CPL and the undesirable effects cited above do not apply here. Also, the error bars on the S_3 measurement are negligible and do not increase those of b_1.

Table 1 GC × GC-TOFMS analysis of the supplied fenchone samples, along with the relative ee measured by PECD

	GC × GC-TOFMS			PECD
Sample	Enantiomeric excess (%)	Chemical purity[b] (%)	$\lvert ee_R/ee_S \rvert$	$\lvert ee_R/ee_S \rvert$
R-(+)-Camphor	+96.7 ± 0.9[a]	>99.9	0.979(9)[a]	0.97(2)[c]
S-(−)-Camphor	−98.7 ± 0.1[a]	>99.9		
R-(−)-Fenchone	+82.1 ± 0.5[a]	>99.9	0.821(5)[a]	0.82(1)[c]
S-(+)-Fenchone	−99.90 ± 0.03[a]	>99.9		

[a] 3σ error bars. [b] Not considering non-volatile or solvent species. [c] 1σ error bars.

The data shown in Fig. 1 and 2 can be obtained at different photon energies in order to study dynamical effects such as the dependence on electron kinetic energy or the effects of continuum resonances. For this, the orbital-specific PECD has been extracted by taking the PES intensity weighted average of b_1 over the FWHM of the corresponding electronic band. The results are given in Fig. 3 and 4 for the HOMO and HOMO−1 of camphor, which also compile the data from previous works. The HOMO−1 data have been obtained by filtering the electron images on the sum of the camphor fragments (discarding therefore the parent contribution) and by considering the binding energy range 10.0–10.3 eV as in ref. 36. Note that for the sake of providing highly accurate benchmarking PECD data, we list in Table 1 of the ESI,† the corresponding new b_1 values.

The new data on the HOMO orbital of camphor, as given by the solid squares in Fig. 3, fit very well with previous existing data recorded below 10 eV and above 13 eV although they have much better accuracy. The completion of the 10–13 eV photon energy range is extremely useful since in this range the CMS-Xα model[36] made predictions of oscillations in the PECD which are now clearly evident in the experimental data. While these fixed equilibrium geometry calculations appear to overemphasize the magnitude of the swings experimentally observed in the 10–17 eV range, they do capture the essence of the energy dependent variation in b_1. One may speculate that allowance for vibrational motion averaging in such calculated PECD might attenuate the swing in b_1 values suggested by experiment. An alternative calculation, the density functional based B-spline model of Stener *et al.*[41] has previously been reported and compared. In the case of core shell C1s ionization of camphor, both models give very comparable results in close agreement with the experimental data.[41] Unfortunately, due to limitations in the LB94 exchange–correlation potential employed for these B-spline calculations the scattering potential generated for the valence ionization was too attractive, and consequently the available B-spline model predictions do not cover this crucial first few eV above the HOMO ionization threshold.

